Journal of Power Sources 214 (2012) 208–215

Contents lists available at SciVerse ScienceDirect

Journal of Power Sources

journal homepage: www.elsevier.com/locate/jpowsour

Improvement of hydrogen storage characteristics of Mg/Mg_2Ni by alloying: Beneficial effect of In

J. Cermak*, L. Kral

Institute of Physics of Materials, v.v.i., AS CR, CEITEC IPM, Zizkova 22, CZ-61662 Brno, Czech Republic

ARTICLE INFO

Article history:
Received 8 February 2012
Received in revised form
10 April 2012
Accepted 17 April 2012
Available online 24 April 2012

Keywords:
Magnesium alloys
Hydrogen desorption
Hydrogen storage
Hydrogen storage materials

ABSTRACT

In the present paper, hydrogen desorption from hydrided binary alloys Mg–*x*Ni (x = 8.5, 11.3, 20 at. %) and from hydrided alloys Mg-8.5 Ni-2.7 *X* (X = Si, Ge, Sn and In; all in at. %) was investigated. It was observed that the phase composition of hydrided binary Mg–*x*Ni alloys changed within several days after hydridation and that rapid hydrogen desorption occurred after this ageing. The ageing mechanism was clarified and its kinetics was modified by alloying. The best results were achieved by adding In: (i) the ageing process was accelerated, enabling rapid hydrogen charging/discharging cycling (ii) the storage capacity was improved slightly, and (iii) the activation enthalpy of hydrogen desorption was decreased, resulting in easier hydrogen releasing.

1. Introduction

There are numerous reviews summarizing the broad class of hydrogen storage materials (HSMs), e.g. [1]. Among the prospective HSMs, Mg-based alloys seem to be of an on-going interest [2,3]. Ball milling [2] and catalysis [4–6] are effective techniques used to improve hydrogen storage characteristics of pure Mg. The mechanism of catalytic action and the effective loci of catalyst atoms were studied in papers [7,8]. Transition metals [9–11] and their oxides [12–16] were used as catalyst. The most efficient addition element was Ni.

Most usually, alloying elements with relatively strong affinity to hydrogen were tested, but hydride non-forming elements may also improve the hydrogen desorption characteristics of HSMs [17–22]. Elements of the 13th (X^{13}) and 14th (X^{14}) groups can be quoted as an example since they form no stable solid hydrides. The hydrides of X^{13} are usually called *polymeric*, because they create chains $(X^{13}H_3)_x$ and their detail structure is unknown [23,24]. The stability of covalent hydrides formed by X^{14} (silane, germanane, stannane and plumbane) is also low and decreases moving down the group in the periodic table.

The present work continues our previous measurements of hydrogen diffusivity in binary alloys Mg–Ni [25], study of catalytic effects [26] and chemical composition of ternary Mg–Ni–*X* alloys, where *X* are elements from the 13th and 14th groups [27]. We observed that sufficient intensity of hydrogen desorption that can be of interest for practical applications, occurred after a certain time at temperatures below some 575 K. This incubation period increased with decreasing desorption temperature. It can slow-down the hydrogen charging/discharging cycles, which is an unpleasant limitation of hydrogen storage solid-state reservoirs with Mg–Ni based alloys. Therefore, we make an attempt to shorten the incubation by modification of the Mg–Ni binary alloy base with the third element.

In the present paper, the phase composition of hydrogen-charged Mg–Ni (–*X*) alloys and their ageing after the hydrogen charging was studied. Chosen elements from the 13th and the 14th groups that form substitution solid solution with the Mg–Ni base (X = Si, Ge, Sn and In) were tested as alloying elements. The remaining elements from the 13th and the 14th groups were disregarded in the present study either due to their extreme toxicity that would limit the applicability of the alloy in technical practice (Tl), due to their propensity to form very stable parasite intermetallics with Ni that decrease the hydrogen storage efficiency (Al, Ga), or due to their high affinity to oxygen because their oxides slow-down the hydrogen transfer inside/outside the HSM (Al, Pb).

2. Experimental

2.1. Experimental alloys – preparation and thermal treatment

Samples were prepared in ball-mill *Fritsch Pulverisette6* using fine splinters of pure Mg (typical thickness was about 100 μm,

* Corresponding author. Tel.: +420 532 290 422; fax: +420 541 218 657.
E-mail address: cermak@ipm.cz (J. Cermak).

0378-7753/$ – see front matter © 2012 Elsevier B.V. All rights reserved.
doi:10.1016/j.jpowsour.2012.04.035

purity 99.98%), Ni powder (grain size 3–7 μm, purity 99.9%) and elements *X* (purity better than 99.99%). The mass ratio of the milling balls to the milled blend was about 60 and the milling cycle – 10 min milling/50 min cooling – was repeated 20 times.

Three binary alloys with average chemical composition of Mg-8.5 Ni (below eutectic – BE), Mg-11.3 Ni (eutectic – E) and Mg-20 Ni (above eutectic – AE), and four ternary alloys of Mg – 8.6 Ni – 2.7 *X* (*X* = In, Si, Ge, Sn; all in at. %) were prepared. The ball-milled powder was compacted at room temperature into cylindrical pellets of a diameter of 20 mm and a height of 4 mm. The pellets were annealed in Ar (purity 99.9999%) at 630 K for 20 h. The annealing was carried out under the Ar pressure of 2 mbar to suppress the oxidation and to prevent the Mg evaporation.

The structure of the samples was observed by SEM JEOL JSM 6460 equipped with the EDAX/WEDAX Oxford Instruments analyzer. XRD patterns were obtained by the X'Pert Pro MPD device using CoKα radiation and the results were interpreted (Rietveld analysis) by the HighScore Plus SW with ICSD databases [28]. The phase analyses were carried out in two states: after stabilization anneal at 630 K/20 h (state A) and after stabilization anneal and hydrogen charging (state B).

2.2. Hydrogen charging and desorption

Samples were hydrided by annealing in gaseous hydrogen (purity 99.9999%, pressure 30 bars) at a temperature of 620 K for 20 h. In a series of hydrogen charging experiments, it was verified that longer charging times did not lead to a higher content of hydrogen.

Desorption of hydrogen was measured in isothermal regime in a Sieverts-type apparatus that was described in detail elsewhere [25]. The pressure $p(t)$ of desorbed hydrogen at desorption time t was measured by a piezoelectric gauge with a sampling frequency of 10 s. Knowing the volume of the desorption chamber (about 5 l) and desorption temperature, the mass of desorbed hydrogen was calculated. The mass of each individual sample was chosen so that the final total hydrogen pressure in the chamber was well below the equilibrium pressure of hydrogen of respective hydrides [29].

The desorption temperature of the sample (556 K–629 K) was measured by a Pt/Pt-10Rh thermocouple that was in contact with the sample and the temperature was stabilized within ±1 K. The samples were moved into the hot zone of the tempered furnace at the beginning and returned into the cold zone after the end of the anneal so that the initial and final temperature changes of the sample were always very short compared to the desorption time period needed for the total isothermal hydrogen desorption. The hydrogen storage capacity was measured by precise weighing of samples, whose total mass was about 2 g.

Measurement of desorption curves $p(t)$ was done immediately after the hydrogen charging (at ageing time τ_0) and, subsequently, it was repeated several times after ageing for time τ at room temperature. The repeating was carried out with different samples of the same alloy.

3. Results and discussion

3.1. Binary alloys

3.1.1. Incubation time of desorption

It was observed that hydrogen desorption curves measured with binary Mg–*x*Ni alloys BE, E and AE changed after hydriding. The change was very expressive at low temperatures below approximately 570 K. Hydrogen desorption measured immediately after hydriding (ageing time τ_0) proceeded very slowly at the beginning of the isothermal desorption test, but after a certain incubation time t_b, the hydrogen evolution was accelerated considerably. The time t_b was reduced markedly during ageing at room temperature for a certain time τ.

Due to a lack of experimental data on low-temperature hydrogen desorption from hydrogen-charged Mg/Mg_2Ni(–*X*) alloys, it is difficult to compare our observation of ageing with the literature. Nevertheless, this effect is similar to hydrogen desorption plateau in Mg modified slightly by various catalysts at temperatures below 573 K, reported in [30,31]. At 573 K and for lower milling times of Mg and Mg_2Ni, a transition was observed [32] to more or less sigmoid-shaped hydrogen desorption curves with very slow hydrogen desorption at the beginning and rapid desorption tail at the end of hydrogen desorption. This is typical for a kind of ageing where initial stage is controlled by nucleation. In some cases, non-regular or non-monotonous hydrogen release from Mg_2Ni at low temperatures was reported [33,34] and not explained as yet.

In Fig. 1, the break point t_b, separating the slow and rapid desorption from BE and AE, is marked by dashed verticals. It can be seen that the incubation time t_b is greater for BE than for AE because AE contains more of Mg_2NiH_4 phase, which catalyses the hydrogen desorption [26]. It is obvious from Fig. 1 that t_b decreases dramatically after ageing at room temperature in the air. The fully aged state was achieved after ageing time τ of about 9 days – longer ageing (τ_∞) led to no significant change of desorption curves more. Interestingly, the total amount of desorbed hydrogen does not depend on ageing time τ. The dependence of desorption curve shape on desorption temperature *T* is shown in Fig. 2. One can see that the break point decreases with increasing *T*.

3.1.2. Mechanism of ageing

The XRD study of hydrided binary Mg–Ni alloys revealed that the phase composition changed during the first several days after the hydriding. The typical XRD pattern is illustrated in Fig. 3. The main phases present in hydrided BE, E and AE alloys were MgH_2, and Mg_2NiH_4 (both low-temperature phases of Mg_2NiH_4, LT1, LT2 [35], were indicated). Also a certain amount of α-solid solution

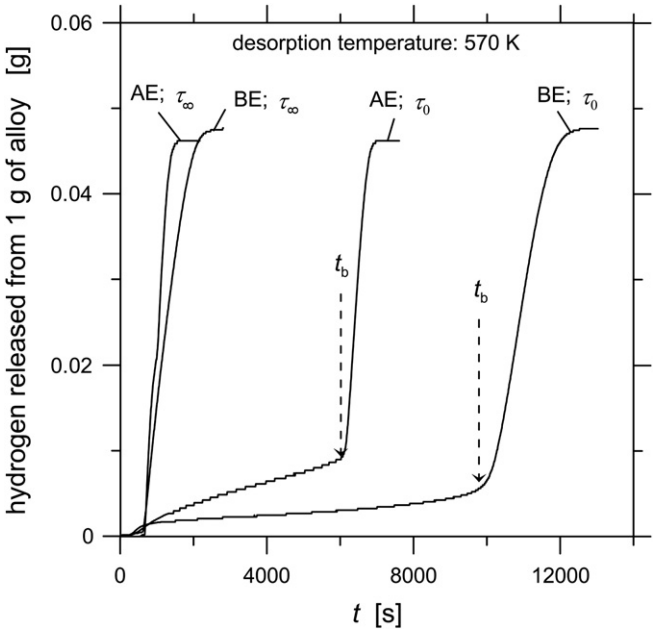

Fig. 1. Desorption curves of hydrided binary Mg–Ni alloys BE and AE measured immediately after hydrogen charging (at ageing time τ_0) and in fully aged state (τ_∞) at a desorption temperature of 570 K t_b – incubation time.

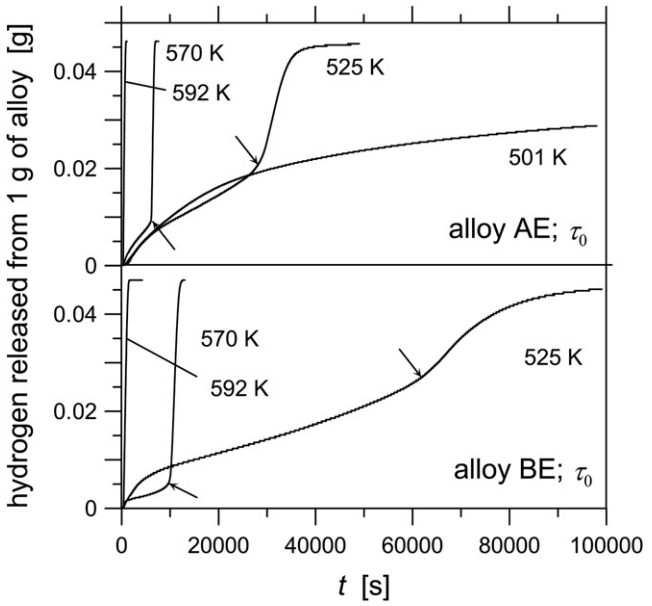

Fig. 2. Desorption curves of hydrided binary Mg–Ni alloys BE and AE measured immediately after hydrogen charging at various desorption temperatures. Arrows – break points at t_b.

$Mg_2NiH_{0.3}$ was always detected (the weight ratio of Mg_2NiH_4/$Mg_2NiH_{0.3}$ was about 6).

The time dependence of phase composition was studied with alloy E. The results obtained by Rietveld analysis for τ_0 (immediately after the hydriding) and for $\tau = 2, 5, 7$ and 9 days are plotted in Figs. 4 and 5. It can be seen in Fig. 4 that the ratio of Mg_2NiH_4/MgH_2 showed a tendency to a slight increase with increasing τ and the low-temperature Mg_2NiH_4 phase was gradually enriched on the non-microtwinned modification LT1 during the first several days after hydrogen charging.

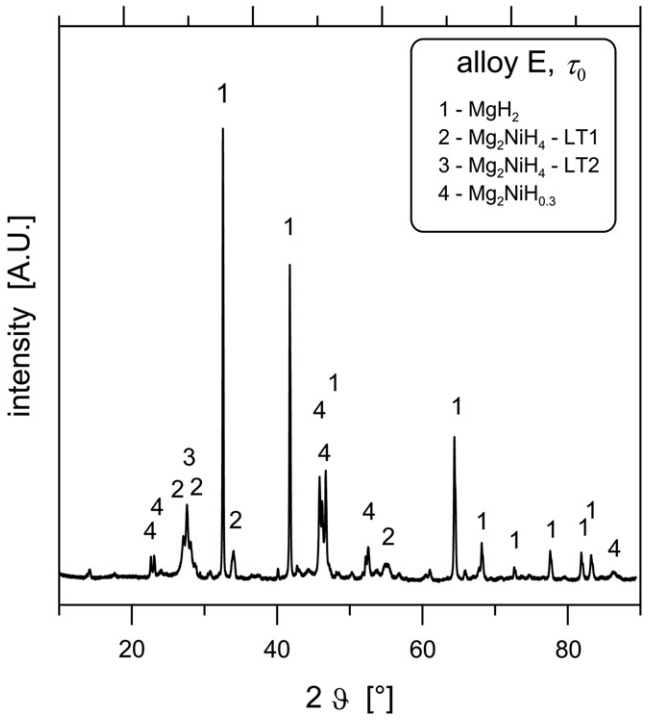

Fig. 3. Example of XRD pattern (alloy *E* measured immediately after hydrogen charging).

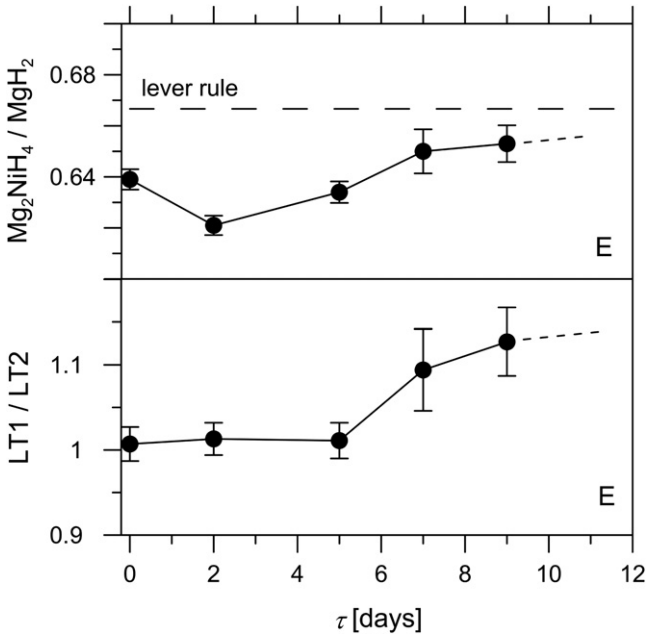

Fig. 4. Phase weight ratios in dependence on ageing time τ; hydrided alloy *E*. Dashed horizontal – calculated from tie-triangle in equilibrium diagram of ternary Mg–Ni–H alloy system.

In Fig. 5, it is shown that the ratios of (Mg)/$Mg_2NiH_{0.3}$ and (Mg)/MgH_2 increased with increasing time of ageing. There is considerable scatter of experimental points, which is given by the fact that the content of (Mg) phase is relatively small. Therefore, e.g., the error originating in inappropriate subtraction of XRD background may contribute to the observed scatter of points. The results in Fig. 5 documented qualitatively the increasing tendency of respective phase ratio with the ageing time.

The observed dependence of phase ratios on time τ can be rationalized by the change of phase composition during the ageing: The structure of hydrided samples and its evolution is illustrated in Fig. 6a, b. Large grains of MgH_2 (grain size 20–50 μm) can be seen

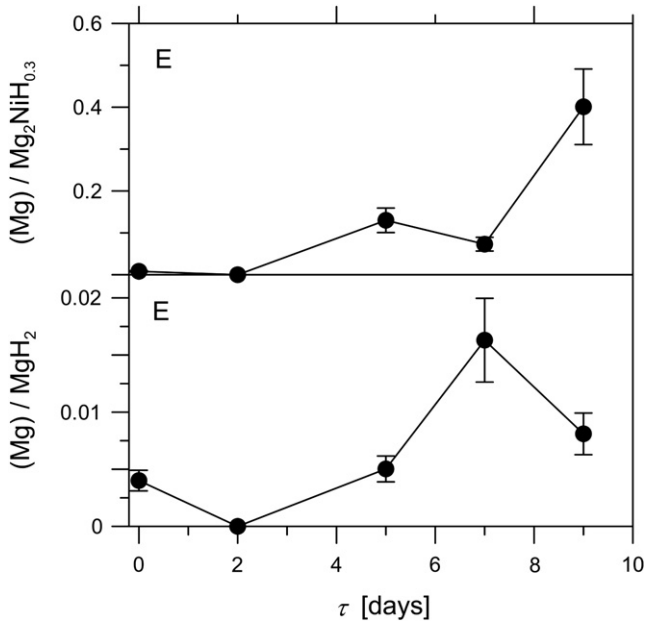

Fig. 5. Phase weight ratios in dependence on ageing time τ; hydrided alloy *E*.

with smaller particles (2–5 μm) of $Mg_2NiH_{0.3}$ and Mg_2NiH_4 on the surface. Hydrogen-saturated hydride Mg_2NiH_4 (β) appears as lighter particles, islands of hydrogen solid solution $Mg_2NiH_{0.3}$ (α) are darker. Reliable identification of both components was done using samples with thinner carbon cover: α-solid solution shows a metallic conductivity, whereas β hydride shows semiconducting to insulating behaviour [36]. It follows from the XRD results (Figs. 4 and 5) that a relatively small fraction of α-solid solution $Mg_2NiH_{0.3}$ transforms to Mg_2NiH_4 hydride. During this transformation, however, hydrogen is consumed. Bearing in mind that the total amount of hydrogen does not change during the ageing (see Figs. 1 and 2), the neighbouring MgH_2 grain must serve as a hydrogen source. It can be supposed that as an inevitable consequence of this hydrogen redistribution, a layer of α-solid solution of hydrogen in magnesium (Mg) was formed in the vicinity of the original interface of $MgH_2/Mg_2NiH_{0.3}$ (Fig. 6b). The resulting structure generated *in situ*, i.e. without exposition to air, was as follows (see the inset in Fig. 6b): [Large MgH_2 grain–(Mg)–Mg_2NiH_4]. Since it is known that Mg_2NiH_4 particles and Mg isles act as a gate of easy transport of hydrogen from MgH_2 [26,37], and bearing in mind that especially LT1 is an effective catalyst for hydrogen desorption [26], it is most likely that the resulting structure generated during the ageing in the vicinity of original $MgH_2/Mg_2NiH_{0.3}$ interface is the cause of earlier onset of rapid hydrogen desorption, which was demonstrated by decreased value of t_b after ageing.

3.2. Ternary alloys

3.2.1. Addition of the third element

The incubation period slows-down the hydrogen charging/discharging cycles during the service of HSM. This is a serious disadvantage that inhibits technical applications of the Mg–Ni binary base especially at reasonably low operation temperatures (below some 500 K). We made an attempt to shorten the long incubation time before the onset of rapid hydrogen discharging at low temperatures by an introduction of third elements from the 13th and 14th groups to Mg–*x*Ni binary alloys. It was found in the previous paper that all tested elements enter the Ni-containing phase preferentially [27].

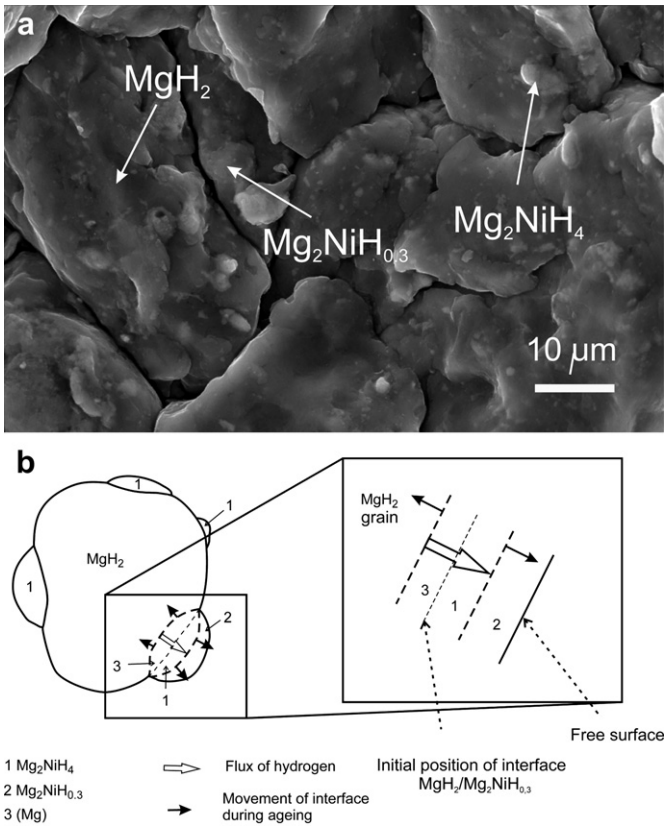

Fig. 6. SEM micrograph of hydrided alloy *E* (a), mechanism of ageing – see text (b).

Desorption curves measured immediately after hydridation (at time τ_0) are shown in Fig. 7a–e where they are compared with desorption curves measured with non-alloyed binary basis Mg-11.3 at.% Ni (NA; alloy E). It is obvious that all tested elements *X* decrease time t_b, at low temperatures 556 K and 575 K.

It can be also seen that the hydrogen storage capacity (maximum amount of hydrogen desorbed from 1 g of fully hydrogen-charged Mg–Ni–*X* alloy) was modified by *X*: The lowest storage capacity was observed in Mg–Ni–Si, the highest capacity (even higher than in NA) was achieved in Mg–Ni–In.

3.2.2. Results of XRD measurement

The XRD patterns of studied ternary alloys in states A and B are shown in Fig. 8a–d and the results of Rietveld analysis are summarized in Table 1. It can be seen that additive elements *X* stabilized the Mg_2Ni phase, which is in agreement with ref [27]. The presence of *X* decreased the Mg_2NiH_4/MgH_2 ratio in state B: the values of the ratio lie in the interval from 0.22 to 0.52 (cf. values of the ratio for binary alloys in Fig. 4). It is also obvious that elements *X* impeded hydridation of Mg_2Ni: The weight ratio of $Mg_2NiH_4/Mg_2NiH_{0.3} < 1$ in state B of Mg–Ni–*X* alloys (average value of about 6 was obtained with binary alloys Mg–Ni in state B).

The weight concentration of indicated phases, *c*, listed in Table 1 was determined with a typical error of about 5%, but in case of small concentrations, absolute error of about 1 wt. % limited the analysis. In the light of this fact, the concentration of Mg_2NiH_4 phase calculated in state B of Mg–Ni–Si and in Mg–Ni–Ge should be taken as a qualitative result only indicating the likely presence of the phase. Within the uncertainty of values *c* mentioned above, the most likely phase transformation occurring during hydridation could be assessed (see Table 1). It seems that Mg and Mg_2Ni phases transformed exclusively into MgH_2 and into a mixture $Mg_2NiH_{0.3} + Mg_2NiH_4$, respectively. Elements X^{14} formed Zintl phases Mg_2X^{14} and ternary intermetallics $Mg_pNi_qX^{14}_r$. They may solve X^{14} partially [38], but they did not take part extensively in hydriding (Table 1).

3.2.3. Influence of air residuals

To assess the influence of residual air in hydrogen on the hydrogen storage characteristics, hydriding of samples was done in two regimes: (i) A closed pressure vessel of the hydriding furnace with samples was filled with hydrogen and pressurized to a total pressure of 31 bar. Hence, the samples were hydrogen-charged in a mixture of air/hydrogen = 1/30. This way of hydridation is referenced as "charging with air" hereafter. (ii) A pressure vessel was evacuated three times to a total pressure of 10^{-1} mbar and pressurized to 10 bars and, finally, pressurized to a total pressure of 30 bar of H_2. This way of hydridation is referenced as "charging in hydrogen".

The obtained results are listed in Table 2. It can be seen that (i) alloys with In showed the highest hydrogen storage capacity $c^{H_2}_{max}$ and (ii) the presence of air lowered significantly the hydrogen storage capacity of all experimental alloys. The influence of air residuals upon the c_{max} shown in Table 2 suggested to introduce an index of corrosion resistance, ICR = $c^{air}_{max}/c^{H_2}_{max}$ that scales the sensitivity of respective hydrogen storage alloy to the presence of air during the hydrogen charging. The value of ICR = 1 indicates no sensitivity to air residuals in hydrogen, small values of ICR << 1, on

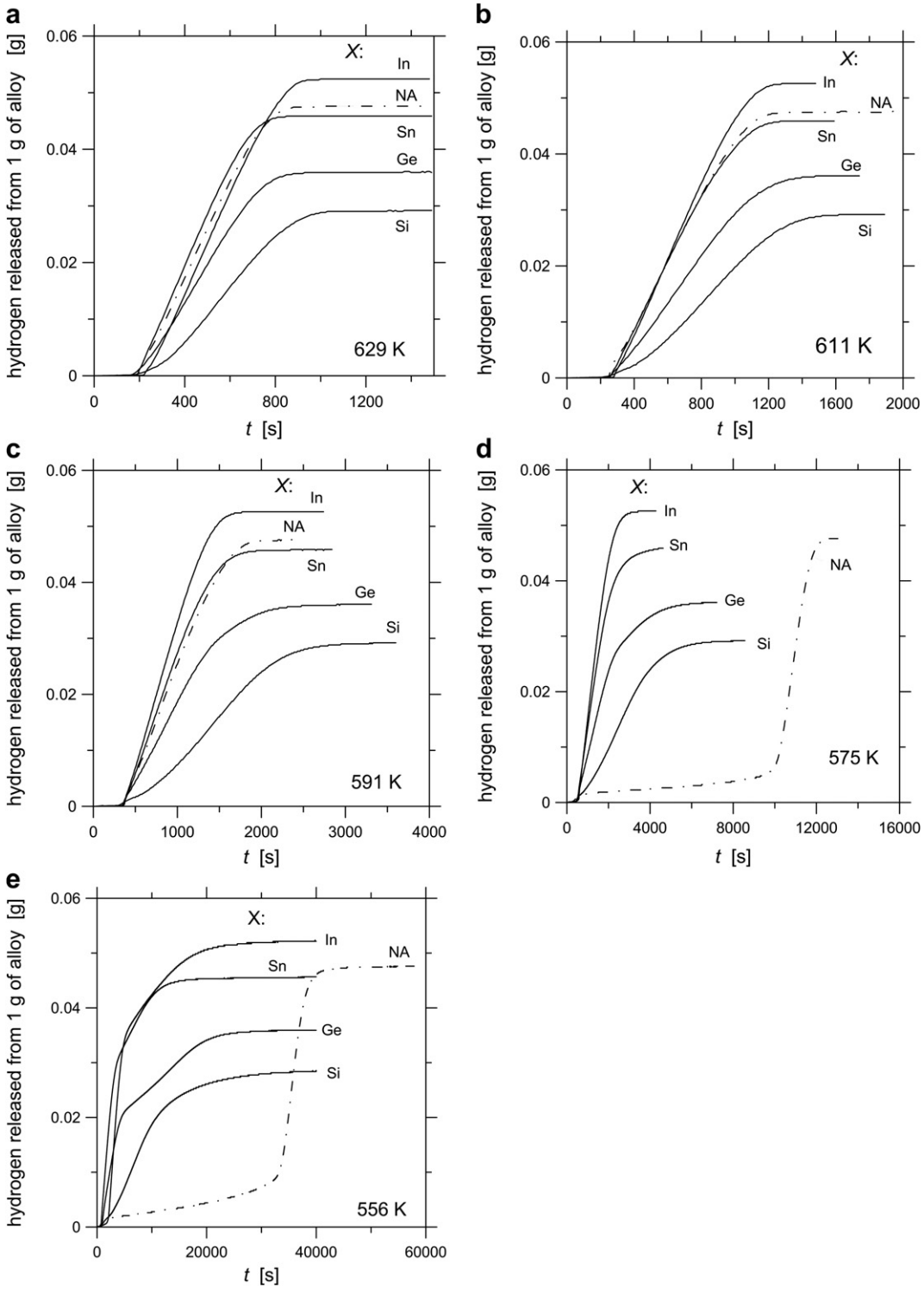

Fig. 7. Desorption curves measured with hydrided ternary Mg–Ni–*X* alloys at temperatures of 629 K (a), 611 K (b), 591 K (c), 575 K (d), 556 K (e). NA – non-alloyed binary *E* alloy.

the other hand, indicate high sensitivity to poisoning of the HSM by air residuals in hydrogen. It is obvious from Table 2 that In showed optimum results: Compared to a non-alloyed material (NA), it increased $c_{max}^{H_2}$ and kept a relatively high poisoning resistance.

3.2.4. Activation enthalpy of hydrogen desorption

A method described in our earlier paper [25] was applied to evaluation of hydrogen diffusion coefficient *D*. Only desorption curves measured at three highest desorption temperatures, where the desorption process can be characterized by a single effective diffusion coefficient *D* (no incubation) were fitted to analytic solution. The arrhenius diagram of the calculated values of *D* is shown in Fig. 9 and calculated activation enthalpies *Q* are listed in Table 2. It is clear that In lowers the value of *Q* and, therefore accelerates the hydrogen desorption rate.

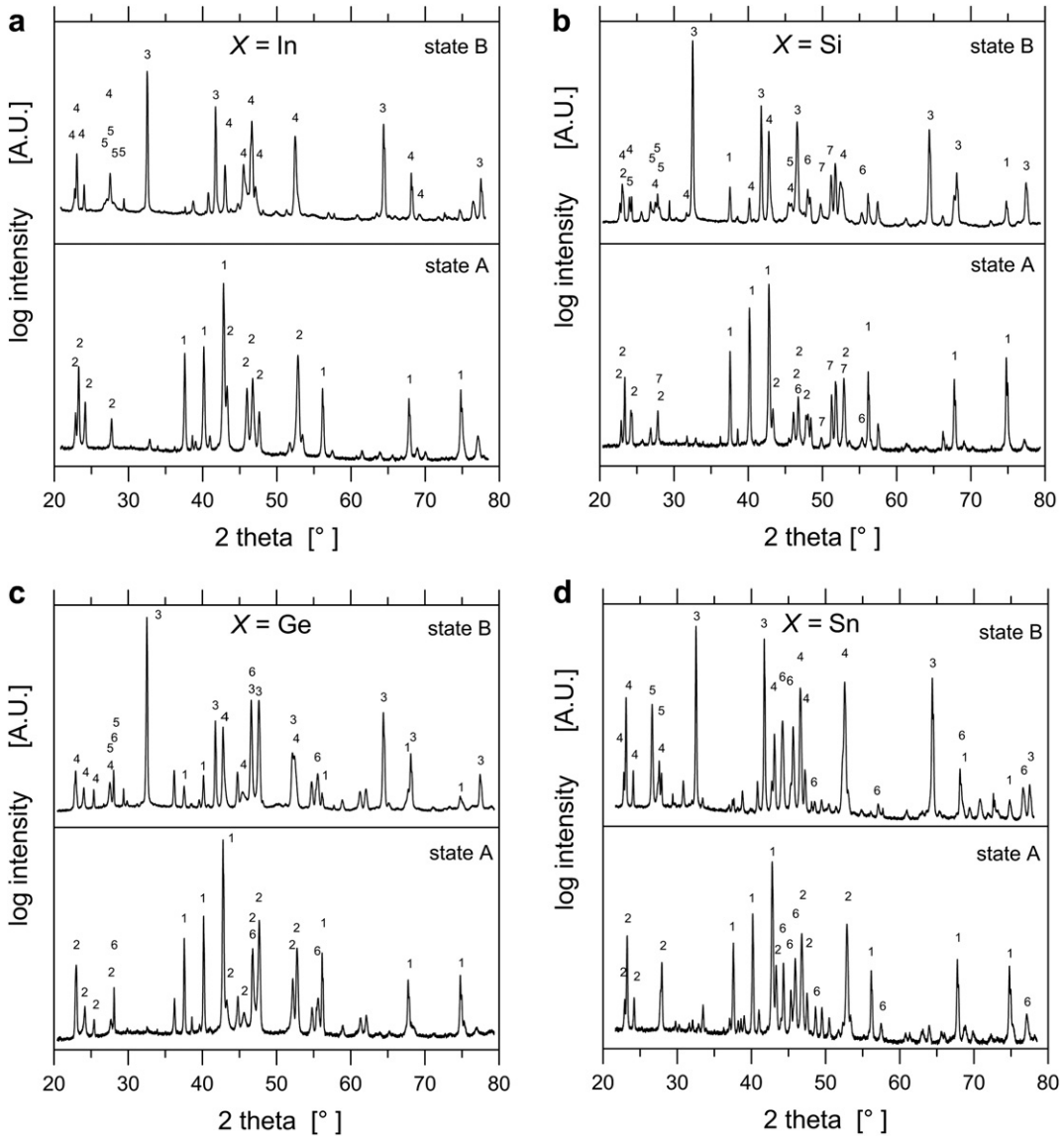

Fig. 8. XRD patterns measured with ternary Mg–Ni–*X* alloys in states A and B. 1 – (Mg), 2 – Mg_2Ni, 3 – MgH_2, 4 – $Mg_2NiH_{0.3}$, 5 – Mg_2NiH_4. (a): *X* = In; (b): *X* = Si, 6 – Mg_2Si, 7 – Mg_2Ni_3Si; (c): *X* = Ge, 6 – Mg_2Ge; (d): *X* = Sn, 6 – $Mg_{79}Ni_{13}Si_8$.

Table 1
Phase composition in ternary Mg–Ni–*X* alloys.

Group	*X*	State A		State B		Phase transformation during hydriding
		Phase	*c* [wt. %]	Phase	*c* [wt. %]	
13	In	Mg	66	MgH_2	66	$Mg \rightarrow MgH_2$
		Mg_2Ni	34	$Mg_2NiH_{0.3}$	25	$Mg_2Ni \rightarrow Mg_2NiH_{0.3} + Mg_2NiH_4$
				Mg_2NiH_4	9	
14	Si	Mg	73	MgH_2	73	$Mg \rightarrow MgH_2$
		Mg_2Ni	19	$Mg_2NiH_{0.3}$	16	$Mg_2Ni \rightarrow Mg_2NiH_{0.3} + Mg_2NiH_4$
		Mg_2Si	5	Mg_2NiH_4	1	$Mg_2Si \rightarrow Mg_2Si$
		Mg_2Ni_3Si	4	Mg_2Si	4	$Mg_2Ni_3Si \rightarrow Mg_2Ni_3Si$
				Mg_2Ni_3Si	6	
	Ge	Mg	70	MgH_2	68	$Mg \rightarrow MgH_2$
		Mg_2Ni	27	$Mg_2NiH_{0.3}$	27	$Mg_2Ni \rightarrow Mg_2NiH_{0.3} + Mg_2NiH_4$
		Mg_2Ge	3	Mg_2NiH_4	1	$Mg_2Ge \rightarrow Mg_2Ge$
				Mg_2Ge	5	
	Sn	Mg	58	MgH_2	53	$Mg \rightarrow MgH_2 + Mg$
		Mg_2Ni	30	$Mg_2NiH_{0.3}$	27	$Mg_2Ni \rightarrow Mg_2NiH_{0.3} + Mg_2NiH_4$
		$Mg_{79}Ni_{13}Sn_8$	12	Mg_2NiH_4	5	$Mg_{79}Ni_{13}Sn_8 \rightarrow Mg_{79}Ni_{13}Sn_8$
				Mg	3	
				$Mg_{79}Ni_{13}Sn_8$	12	

Table 2
Hydrogen storage capacity c_{max} in wt. % H_2, index of X segregation IXS in state B, index of corrosion resistance ICR ($c^{H_2}_{max}$ – charged in H_2, c^{air}_{max} – charged with air) and activation energy of hydrogen desorption Q in kJ/mol H_2. NA – non-alloyed material. Average relative errors of c_{max} and Q are 2% and 6%, respectively.

Group	X	IXS[a]	c_{max}		ICR	Q
			c^{air}_{max}	$c^{H_2}_{max}$		
13	In	13.9	2.3	5.3	0.43	47
14	Si	1.0	0.55	2.9	0.19	93
	Ge	2.3	0.45	3.6	0.13	104
	Sn	7.8	1.4	4.6	0.30	80
NA		–	2.7	4.8	0.54	69

[a] [27].

3.2.5. Relation between hydrogen storage characteristics and distribution of X

To summarize the observed effects of X on the hydrogen storage characteristics, it is meaningful to introduce an index of X segregation IXS $= c_X^{Mg_2NiH_x}/c_X^{Mg_2H_2}$, where $c_X^{Mg_2NiH_x}$ is concentration of X in Mg_2NiH_x and $c_X^{Mg_2H_2}$ is concentration of X in MgH_2 [27]. IXS expresses the relative affinity of element X to both phases: higher values of IXS indicate a tendency to enrichment of Mg_2NiH_x (x is either 0.3 or 4) on X, lower values of IXS indicate relative enrichment of MgH_2 phase on X. Values of IXS obtained in the previous paper [27] are shown in Table 2.

It can be seen in Table 2 that Si showed significant affinity to neither of the two phases (IXS = 1), whereas In strongly concentrated in Mg_2NiH_x (IXS ~ 14). The affinity of the other elements, Ge and Sn, lie between these extremes.

Fig. 10 documents that a relatively significant correlation was found between IXS on the one hand and some materials parameters related to hydrogen storage properties on the other: The amount of Mg_2Ni phase detected in ball-milled and annealed samples of Mg–Ni–X (state A) increased with increasing IXS (Fig. 10a), which

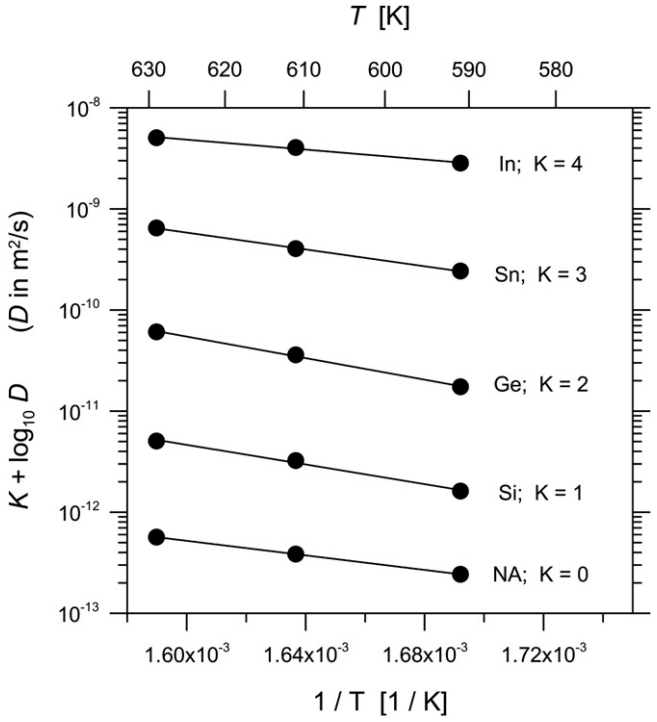

Fig. 9. Arrhenius diagrams of hydrogen diffusion coefficient D. T – desorption temperature, K – additive constant separating experimental points for individual elements X. NA – non-alloyed binary E alloy.

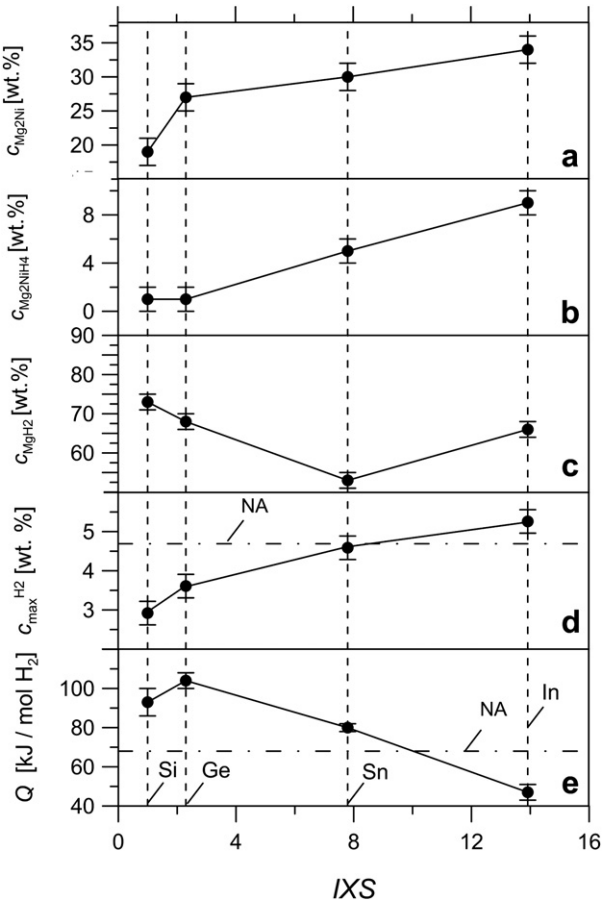

Fig. 10. Dependence of phase concentration of Mg_2Ni (a), Mg_2NiH_4 (b), MgH_2 (c), hydrogen storage capacity $c^{H_2}_{max}$ (d) and activation enthalpy of hydrogen desorption Q (e) on index of X segregation IXS.

can be rationalized by the stabilizing of Mg_2Ni by additives with a higher value of IXS [27].

As mentioned in section 3.2.2, the amount of Mg_2NiH_x phase in ternary Mg–Ni–X alloys was lower than that in binary Mg–Ni alloy, which can also be ascribed to stabilization of non-hydrided state by X. However, it was observed that amount of Mg_2NiH_4 after hydrogen charging was an increasing function of IXS (Fig. 10b). This is also in agreement with even stronger affinity of X to hydrided phase Mg_2NiH_4 reported in [27]. This manifested itself in observed increasing content of the Mg_2NiH_4 phase by elements with increasing index IXS.

Dependence of the amount of MgH_2 phase on IXS, on the other hand, shows a little complicated course with a local minimum for Sn. This may be partly due to the fact that not all amount of Mg phase present in the State A of Mg–Ni–Sn alloy transformed during the hydriding to MgH_2.

It can be shown that the hydrogen storage capacity, $c^{H_2}_{max}$ (maximum hydrogen content in the HSM), was the higher, the higher was index IXS of element X (Fig. 10d). For In, the value of $c^{H_2}_{max}$ was even higher than hydrogen storage capacity of non-alloyed binary alloy Mg–Ni.

It is shown in Fig. 10e that elements with high IXS index reduce the activation enthalpy of hydrogen desorption, Q, which leads to easy hydrogen desorption. For In, the value of Q is even lower than the value for non-alloyed binary Mg–Ni alloy.

Results in Fig. 10 and in Table 2 indicate that In allows to the best hydrogen absorption/desorption characteristics. It stabilizes Mg_2Ni phase and its hydride Mg_2NiH_4, which act as gate for easy hydrogen

transfer from/to MgH_2 [26]. This is in agreement with our previous observation of In distribution between the main phases of hydrided alloys Mg–Ni–*X* [27]. In also imparts the alloy good resistance against the detrimental effect of rest air in hydrogen. Beneficial effect of In on shortening of incubation period of hydrogen desorption at low temperatures, on hydrogen storage capacity c_{max} and on activation enthalpy of hydrogen desorption *Q* may be caused by catalytic behaviour of In: surface locations enriched by In are most likely formed that provide preferred dissociation/recombination sites for hydrogen [39].

4. Conclusions

The obtained results can be summarized as follows:

The phase analysis of hydrogen desorption from binary Mg–*x*Ni alloys led to a conclusion that the incubation period of rapid hydrogen desorption is a time needed for phase transformation of $Mg_2NiH_{0.3}$ particles (incompletely hydrided phase Mg_2Ni located on great MgH_2 grains) into Mg_2NiH_4. During this transformation, bridges of easy transfer of hydrogen from MgH_2 are created.

Introduction of the third element *X* (*X* = Si, Ge, Sn and In) into binary Mg–Ni alloy influences considerably the phase composition of the mixture: stabilization of Mg_2Ni phase by all elements *X* causes that the fracture of $Mg_2NiH_{0.3}$ is markedly increased. This leads to an increase in the number of potential bridges of easy desorption and therefore, to a shorter incubation period of easy hydrogen desorption t_b. Beneficial effect showed, above all, elements *X* with a high affinity to Mg_2NiH_x phase. The most advantageous is alloying of Mg–Ni with In. In the light of our previous paper, during time period t_b sufficient number of catalyzing sites is generated that accelerate the hydrogen desorption. It was found that In promotes the process very effectively.

The hydrogen storage capacity of Mg–Ni–In alloy is higher than the capacity of non-alloyed Mg–Ni and the activation enthalpy of hydrogen desorption *Q* is lower than that of non-alloyed Mg–Ni. Moreover, In does not significantly spoil the resistivity of non-alloyed Mg–Ni against the poisoning by air residuals in hydrogen.

Acknowledgements

This work was supported by projects GACR 106/09/0814, GACR P108/11/0148, AV 0Z20410507 and CEITEC CZ.1.05/1.1.00/02.0068. The authors are very grateful to Mr. B. David for assistance with the XRD measurement.

References

[1] G. Sandrock, J. Alloys Compd. vols. 293–295 (1999) 877–888.
[2] B. Sakintuna, F. Lamari-Darkrim, M. Hirscher, Int. J. Hydrogen Energy 32 (2007) 1121–1140.
[3] I.P. Jain, C. Lal, A. Jain, Int. J. Hydrogen Energy 35 (2010) 5133–5144.
[4] P. Larson, C. Moyses-Araujo, J.A. Larson, P. Jena, R. Ahuja, PNAS – Appl. Phys. Sci. 105 (2008) 8227–8231.
[5] S. Li, P. Jena, R. Ahuja, Phys. Rev. B (74) (2006) Article ID 132106 4 pages, doi:10.1103/PhysRevB.74.132106-4.
[6] A. Zaluska, L. Zaluski, J.O. Stroem-Olsen, Appl. Phys. A 72 (2001) 157–165.
[7] A. Montone, A. Aurora, D.M. Gatia, M.V. Antisari, Scripta Mater. 63 (2010) 456–459.
[8] M.V. Antisari, A. Aurora, D.M. Gatia, A. Montone, Scripta Mater. 61 (2009) 1064–1067.
[9] C. Milanese, A. Girella, G. Bruni, P. Cofrancesco, V. Berbenni, P. Matteazzi, A. Marini, Intermetallics 18 (2010) 203–211.
[10] R.W. Denis, I.Yu. Zavaliy, V. Paul-Boncour, V.V. Berezovets, I.V. Kovalchuk, A.B. Riabov, Intermetallics 18 (2010) 1579–1585.
[11] N. Bazzanella, R. Checchetto, A. Miotello, J. Nanomaterials (2011) Article ID 865969 11 pages, doi:10.1155/2011/865969.
[12] X.B. Yu, Z.X. Yang, H.K. Liu, D.M. Grant, G.S. Walke, Int. J. Hydrogen Energy 35 (2010) 6338–6344.
[13] R.R. Shahi, T.P. Yadav, M.A. Shaz, O.N. Srivastva, Int. J. Hydrogen Energy 35 (2010) 238–246.
[14] H. Simchi, A. Kaflou, A. Simchi, Int. J. Hydrogen Energy 34 (2009) 7724–7730.
[15] M. Polanski, J. Bystricki, T. Plocinski, Int. J. Hydrogen Energy 33 (2008) 1859–1867.
[16] F. Tonus, V. Fuster, G. Urretavizcaya, F.J. Castro, J.-L. Bobet, Int. J. Hydrogen Energy 34 (2009) 3404–3409.
[17] M. Tanriu, D.K. Slattery, F. Ebrahimi, Int. J. Hydrogen Energy 35 (2010) 3555–3564.
[18] D.I. Duarte, L.A.C. Bustamante, P.E.V. de Miranda, Scripta Mater. 56 (2007) 789–792.
[19] T. Sato, H. Blomqvist, D. Noreus, J. Alloys Compd. 356–357 (2003) 494–496.
[20] S. Doppiu, P. Solsona, T. Spassov, G. Barkhordarian, M. Dornheim, T. Klassen, S. Surinach, M.D. Baro, J. Alloys Compd. 404–406 (2005) 27–30.
[21] F.C. Gennari, G. Urretavizcaya, J.J.A. Gamboa, G. Mayer, J. Alloys Compd. 354 (2003) 187–192.
[22] F.C. Gennari, F.J. Castro, G. Urretavizcaya, G. Mayer, J. Alloys Compd 334 (2002) 277–284.
[23] G. Brendel, in: Ullmanns Encyklopaedie der technischen Chemie, vol. 13, Verlag Chemie, Weinhaim, New York, 1977, pp. 109–133.
[24] G. Wulfsberg, Principles of Descriptive Inorganic Chemistry, 94965, University Science Books, Sausalito, CA, 1991, 343.
[25] J. Cermak, L. Kral, Acta Mater. 56 (2008) 2677–2686.
[26] J. Cermak, B. David, Int. J. Hydrogen Energy 36 (2011) 13614–13620.
[27] J. Cermak, L. Kral, J. Power Sources 197 (2012) 116–120.
[28] Inorganic Crystal Structure Database (ICSD), Release 2011–2, Fachinformationszentrum Karlsruhe, Germany, and the National Institute of Standards and Technology (NIST), the U.S. Department of Commerce, 2011 United States (CD-ROM).
[29] M. Hirscher (Ed.), Handbook of Hydrogen Storage, Willey-VCH Verlag, Weinheim, 2010, pp. 117–151.
[30] G. Barkhordarian, T. Klassen, R. Bormann, J. Alloys Compd. 364 (2004) 242–246.
[31] G. Barkhordarian, T. Klassen, R. Bormann, Scripta Mater. 49 (2003) 213–217.
[32] R. Janot, X. Darok, A. Rougier, L. Aymard, G.A. Nazri, J.-M. Tarascon, J. Alloys Compd. 404-406 (2005) 293–296.
[33] F.C. Gennari, M.R. Esquivel, J. Alloys Compd. 459 (2008) 425–432.
[34] C.X. Shang, M. Bououdina, Y. Song, Int Z.X Guo, J. Hydrogen Energy 29 (2004) 73–80.
[35] H. Blomqvist, D. Noreus, J. Appl. Phys. 91 (2001) 5141–5148.
[36] S. Enache, W. Lohstroh, R. Griessen, Phys. Rev. B 69 (2004) 115326 (12 pages).
[37] E. Edvard, I. Gabis, V.A. Yartis, Int. J. Hydrogen Energy 35 (2010) 9060–9069.
[38] R. Janot, F. Cuevas, M. Latroche, A. Percheron-Guegan, Intermetallics 14 (2006) 163–169.
[39] Z. Gavra, Z. Hadari, M.H. Hintz, J. Inorg. Nucl. Chem. 43 (1981) 1763–1768.